

Catalysis at the Sub-Nanoscale: Complex CO Oxidation Chemistry on a Few Au Atoms

Nima Nikbin^a, Natalie Austin^b, Dionisios G. Vlachos^{a,}, Michail Stamatakis^{c,*} and Giannis Mpourmpakis^{b,*}*

^a Department of Chemical and Biomolecular Engineering, University of Delaware, Newark, Delaware 19716, USA

^b Department of Chemical Engineering, University of Pittsburgh, Pittsburgh, Pennsylvania 15621, USA

^c Department of Chemical Engineering, University College London, Torrington Place, London WC1E 7JE, UK

Abstract

Au has been widely used as jewelry since ancient times due to its bulk, chemically inert properties. During the last three decades, nanoscale Au has attracted remarkable attention and has been shown to be an exceptional catalyst, especially for oxidation reactions. Herein, we elucidate a puzzle in catalysis by using multiscale computational modeling: the experimentally observed “magic number” CO oxidation catalytic behavior of subnanoscale Au clusters. Our results demonstrate that support effects (cluster charging), symmetry-induced electronic effects on the clusters, catalyst reconstruction, competing chemical pathways and formation of carbonate contribute to the marked differences in the observed catalytic behavior of Au_n clusters with n=6, 8 and 10 atoms. This is the first demonstration of multiscale simulations on subnanoscale catalysts unraveling magic number activity for the CO oxidation reaction on Au.

Keywords

DFT, kinetic Monte Carlo, charge, metal-oxide, support effects

*Corresponding authors: gmpourmp@pitt.edu, m.stamatakis@ucl.ac.uk, vlachos@udel.edu

Introduction

Au is a remarkable metal with unique catalytic properties. It exhibits high activity at the nanoscale¹⁻³, whereas it is inert as bulk material⁴. Because of these unique properties, Au has found applications at both these extreme materials scales. Historically, it has been used as jewelry⁵ since ancient times due to its ability to prevent corrosion in bulk and maintain its bright color. The properties of Au at the nanoscale have recently been revealed with the explosive growth of nanotechnology. Nanoscale Au⁶⁻⁹ finds tremendous applications ranging from drug delivery¹⁰ in medicine to hydrogen production² and energy generation.

Focusing on the catalytic applications of Au and specifically on the relatively simple CO oxidation reaction ($\text{CO} + \frac{1}{2} \text{O}_2 \rightarrow \text{CO}_2$), Haruta first showed that Au nanoparticles¹¹ exhibit exceptional reactivity even at low temperatures¹²⁻¹⁷. These active Au nanoparticles are usually supported on metal-oxide surfaces^{3, 18-20}. Despite the large volume of work focused on the CO oxidation on Au in the last ~30 years, there is still much debate regarding the reaction mechanism²¹. This is due to a large number of factors influencing the catalytic activity, such as the effect of the support, the Au particle size, and the presence of quantum effects in sub-nanometer catalysts. An emerging consensus is that under-coordinated sites on Au nanoparticles are the active sites for oxidation chemistry²²⁻²⁵. The Au nanoparticle sites on the metal-support interface which have been experimentally shown to be catalytically active^{26, 27} can be also considered as under-coordinated sites.

According to this consensus about Au, which suggests “the smaller the size, the higher the activity per site”, we would expect all sub-nanometer, molecular size catalysts to be the most catalytically active. However, CO oxidation experiments involving small Au_n clusters (n= 2-20 atoms, < 1 nm diameter) soft-landed on an O-defective MgO support²⁸⁻³⁰, revealed “magic number” catalytic behavior. The most active clusters were the Au₈²⁹, Au₁₈ and Au₂₀. The activity was attributed to the negative charge transferred from the support-vacancy to the clusters which activates O₂ adsorption^{28, 29}. Previous work has proposed that O₂ binds strongly on Au clusters with an odd number of electrons^{31, 32}. As a result, negatively charged Au clusters with an even number of Au atoms are expected to show increased activity because, in addition to having low-coordinated sites, they also exhibit a preferred electronic configuration for O₂ adsorption and activation³³. This magic number behavior, particularly illustrated by Arenz et al³⁰, is most

probably generic of sub-nanometer catalysis well beyond Au and remains an elusive field of catalytic science^{2, 34, 35}.

In this work we use first-principles-based multiscale modeling to demonstrate that the CO oxidation activity of subnanometer Au is controlled by rather complicated physicochemical processes: charge transfer, different catalyst shapes, cluster reconstruction, electronic density on the catalyst, binding configuration of adsorbates and production of carbonate species can contribute towards the magic number catalytic behavior on Au. Important enough, this work demonstrates the impact of a multiscale theoretical framework, linking *ab-initio* calculations with statistical mechanics, which enables us to access experimental length and time scales of complex catalytic systems.

Computational Methods

The support (MgO) effects on the Au clusters (charge) were calculated at the BP86/def-sv(p) level and default effective core pseudopotentials (def-ecp) were included for Au atoms, using the RI (resolution of identity) approximation as implemented in Turbomole 6.5³⁶. The perfect MgO support consists of 112 atoms, $\text{Mg}_{56}\text{O}_{56}$, whereas the ones with an O vacancy consist of one atom less ($\text{Mg}_{56}\text{O}_{55}$). In these calculations, the MgO was first fully optimized and then, when the clusters (Au_6 , Au_8 and Au_{10}) were supported, the MgO coordinates were kept frozen and the clusters were allowed to fully relax on the MgO surface. Having identified a charge transfer from the support to the clusters, we removed the clusters from the support and we thoroughly investigated the CO oxidation reaction mechanisms on every possible site of the negatively charged clusters (Au_6^- , Au_8^- and Au_{10}^-) at the B3LYP/LANL2DZ level of approximation, using the Gaussian 09 software package³⁷. This combination of method and basis set has been successfully used to investigate the CO oxidation mechanism on Au clusters³⁸⁻⁴⁰. All reaction pathways were first mapped by scanning the potential energy surface of the reaction coordinate. The energy maximum found along the reaction coordinate was fully relaxed to a saddle point in order to locate the actual transition state. All transition states and local minima were obtained by full optimizations and verified by vibrational frequency and Intrinsic Reaction Coordinate (IRC) calculations.

The data from the aforementioned calculations served as input to *Zacros*,⁴¹ our in-house Fortran implementation of the graph-theoretical kinetic Monte Carlo (KMC) simulation

framework^{42, 43}. This input consists of a lattice structure, an energetics model, a reaction mechanism, and finally, the conditions of the simulation along with control parameters such as the frequency of sampling/reporting etc. Three planar lattices were thus used to represent the top and bridge sites of the Au nanoclusters, as shown in Figure 1.

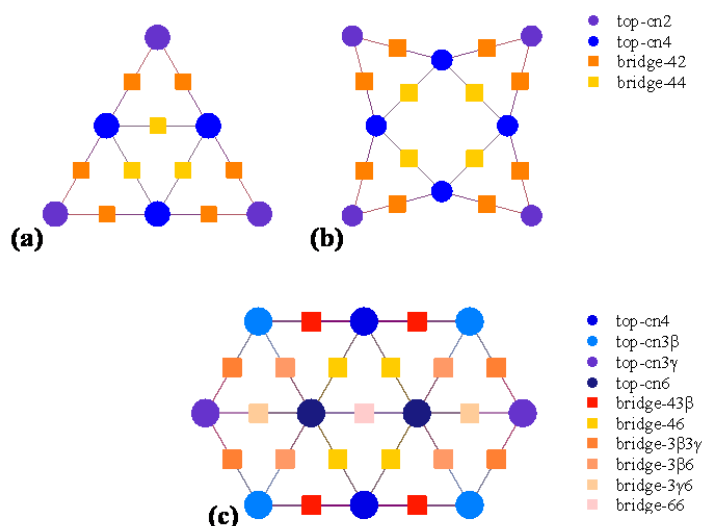


Figure 1: Lattice structures for the three Au nanoclusters, denoting the sites that were taken into account in the models.

The energetics model contained the binding energies of all intermediates to the pertinent sites (top and bridge), and explicitly accounted for multi-site species, such as carbonate. Moreover, strong repulsive interactions between O_2 adsorbates were incorporated into the energetics model, since the DFT calculations showed that a maximum of one oxygen molecule can bind to any of these clusters. All energetics models are presented in detail in the supplementary material.

The reaction mechanism for each of the three nanoclusters contained the adsorption/desorption, diffusion and surface and Eley-Rideal reaction elementary steps computed via DFT. Transition state theory approximations were used to calculate the rate constants (see supplementary material of Ref. ⁴⁴). Within the KMC framework, event occurrence is treated as a Poisson stochastic process, and to simulate the occurrence of the elementary events, *Zacros* utilizes a rejection-free algorithm with local updating of the propensities⁴⁵. In view of the stochastic nature of KMC, ensembles of 100 (for Au_6^-) or 10 clusters (for Au_8^- and Au_{10}^-) were used to investigate the kinetics. All simulations were performed at a temperature of 250 K for an

isomolar mixture of CO and O₂ at 1 bar. It should be noted that we have successfully applied this methodology to the MgO supported Au₆ clusters very recently⁴⁶, by investigating support effects and reaction mechanism with quantum mechanical calculations (RI-BP86 and B3LYP level of approximation respectively) and importing the DFT-calculated reaction energetics into graph-theoretical kinetic Monte Carlo simulations.

Results

Au clusters up to the Au₁₃ size (consisting of 13 atoms) exhibit planar geometries. When these clusters are supported on MgO with O vacancies they are charged negatively^{29, 46}. Each O vacancy can give electron density to the clusters approximately close to one electron (-0.8 to -1.4 |e|), whereas, when the clusters are supported on a perfect MgO the charge that is transferred is significantly smaller (-0.2 to -0.3 |e|). This behavior is illustrated in Figure 2, where we show the interactions of Au₆, Au₈ and Au₁₀ with MgO and the total charge transferred from the support.

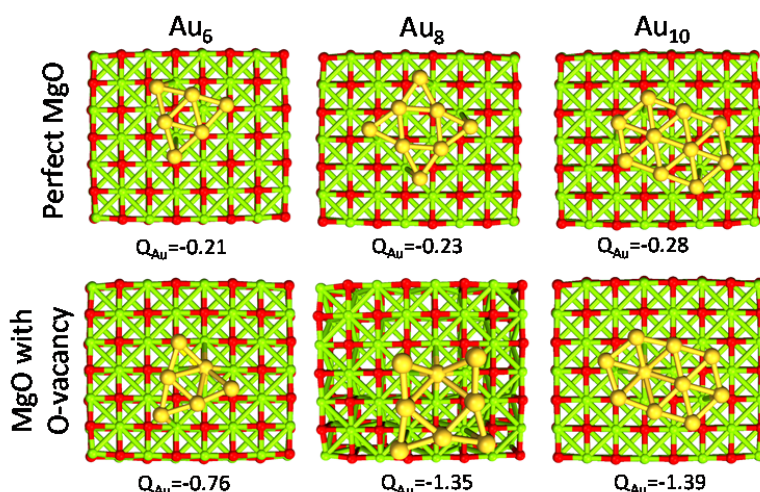


Figure 2: Au₆, Au₈ and Au₁₀ clusters interacting with a perfect MgO support and a support with an O vacancy. The total Natural Bond Orbital (NBO) charge transferred from the support to the clusters is shown at the bottom of each graph.

This electron density can be transferred to the clusters, even when the clusters are 20 Å away from the support vacancy⁴⁷. Clusters with even number of atoms will end up with an odd number of electrons after this electron transfer from the support vacancy, which will favor O₂ adsorption. In Figure 3 we present the HOMO and LUMO (highest occupied and lowest unoccupied molecular) orbitals of the Au₆⁻, Au₈⁻ and Au₁₀⁻ clusters (catalysts of interest). CO (O₂) is an

electron donor (acceptor) molecule and preferentially interacts with sites on the clusters where the LUMO (HOMO) orbitals are localized. The first complexity in these molecular-sized catalysts arises from the fact that the HOMO and LUMO orbitals are not necessarily localized on the lowest coordinated sites of the clusters³². As a result, the lowest coordinated sites are not necessarily the strongest adsorption sites on the catalysts. This is exemplified in the case of Au_{10}^- where the HOMO orbital, which is semi-occupied, is localized primarily on the Au atoms that exhibit coordination number 4 (and to their first neighbors with coordination number 3) and not explicitly to the lowest coordinated sites of the cluster (with coordination 3). Thus, molecular oxygen adsorbs on Au_{10}^- cluster with a bidentate configuration on top of the Au atoms where the HOMO orbital is localized (see initial state in Figure 4(d) *vide-infra*).

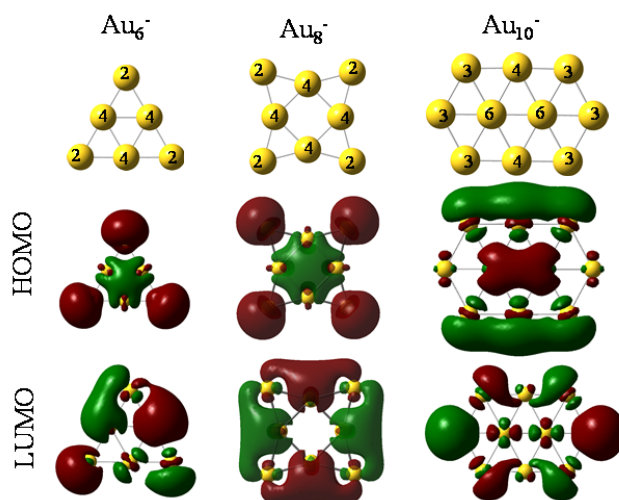


Figure 3: Geometries and molecular orbital density of Au_6^- , Au_8^- and Au_{10}^- clusters. The numbers on the clusters represent the coordination of each Au atom. The highest occupied (HOMO) and the lowest unoccupied molecular orbitals (LUMO) of each cluster are illustrated. The HOMO orbitals are semi-occupied in every case (spin multiplicity doublet).

Next we calculated the detailed energetics of the CO oxidation reaction (step 1: $\text{CO}^* + \text{O}_2^* \rightarrow \text{CO}_2 + \text{O}^*$ and step 2: $\text{CO}^* + \text{O}^* \rightarrow \text{CO}_2$) on these three clusters, by taking into consideration every possible adsorption configuration of CO and O_2 . As a result, we calculated approximately 160 catalytic events which include: adsorption, reaction, and desorption of all the gas species. Details about the calculations and reaction energy pathways appear in the supporting information file. In Figure 4 (a) – (c), we selectively present the first step of the CO oxidation reaction from a 4-center CO- O_2 adsorbed intermediate that has been reported to be the rate

limiting step in the CO oxidation reaction³⁸. These specific reaction steps on each of the three clusters appear to control their reactivity, but for completely different reasons as we will show next with our kinetic Monte Carlo (KMC) simulations. Just by comparing the density functional theory (DFT) calculated reaction barriers on Au_6^- =16.2, Au_8^- =14.8, and Au_{10}^- =13.2 (kcal/mol) presented in Figure 4 (a)-(c), one could conclude that Au_{10}^- appears to be the most active cluster among the three and the activity is a monotonic function of size, in contradiction to experiments. In Au_6^- , the product of the first CO oxidation reaction step is carbonate (CO_3) and not CO_2 . Carbonate binds very strongly on the catalyst and its dissociation to a CO_2 molecule is highly unfavorable⁴⁶. A unique reaction step to the Au_{10}^- case is the O_2 “tilting” presented in Figure 4 (d). O_2 preferentially interacts with the cluster with the bidentate configuration due to electronic reasons we discussed in the previous paragraph. In this configuration, O_2 has to tilt in order to react with CO through the 4-center intermediate, which requires activation energy of 10.7 kcal/mol.

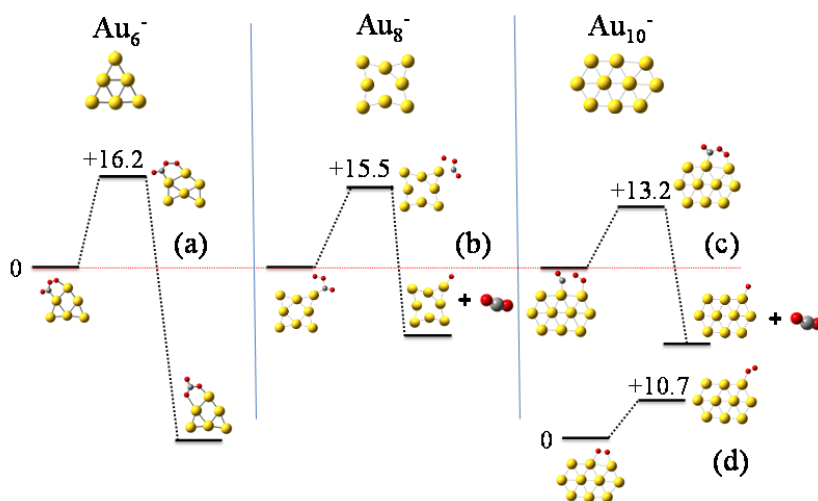


Figure 4: Key reactions controlling catalytic activity on the clusters among 160 total reaction steps investigated by quantum mechanical theoretical calculations: (a) – (c) first step of CO oxidation mechanism involving a CO- O_2 four-center intermediate and on Au_6^- , Au_8^- and Au_{10}^- , respectively, and O_2 tilting step on Au_{10}^- (d).

The reason that carbonate forms on Au_6^- is because the cluster has two almost isoenergetic ($\Delta E \sim 2$ kcal/mol) geometries of D_{3h} and D_{2h} symmetries and can restructure with a very small transformation barrier of ~ 4 kcal/mol. Freezing the cluster in its initial geometry during reaction pathway calculations would result in the formation of CO_2 and not carbonate. Interestingly, as we show in Figure 5, a similar transition from a D_{4h} to a stable geometry of

lower symmetry (e.g., D_{2h}) does not exist in Au_8^- neither on the neutral states of these two clusters (Au_6^0 , Au_8^0). Even though it is possible that reconstruction happens on Au_8^- catalyst under reaction conditions (e.g., adsorbate-induced, see detailed reaction mechanism presented in Figure 7(b)), we show that at least for the specific elongation coordinate (similar to the one causing reconstruction of Au_6) shown in Figure 5 the cluster is stable (i.e., symmetry-induced reconstruction does not occur).

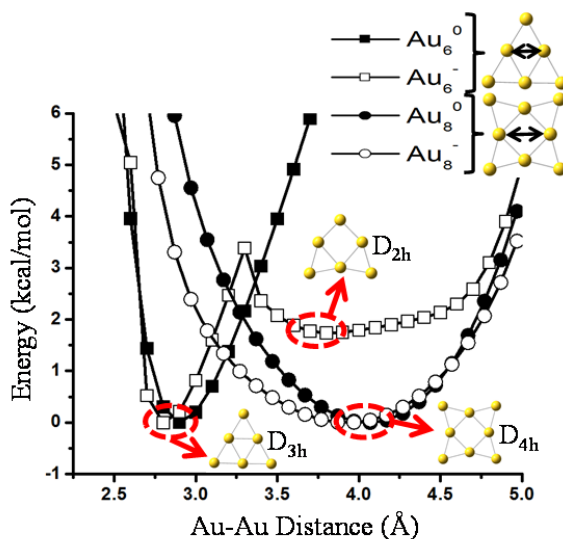


Figure 5: Potential energy curves of Au_6 (squares) and Au_8 (circles) catalyst restructuring in neutral (closed symbols), and negative (opened symbols) charge states. The elongation coordinates are shown in the upper right.

To investigate the reactivity of the three different nanoclusters for the CO oxidation we performed first-principles KMC simulations⁴⁴ using our *ab-initio* data as input and the *Zacros* software implementation of the Graph-Theoretical KMC method^{42, 43}. By calculating the number of CO_2 molecules produced per site per time, we estimated the turnover frequencies (TOFs) for each Au structure, and by analyzing the statistics of occurrence of each elementary step, we identified the dominant pathways for each structure. The results are presented in Figures 6-8.

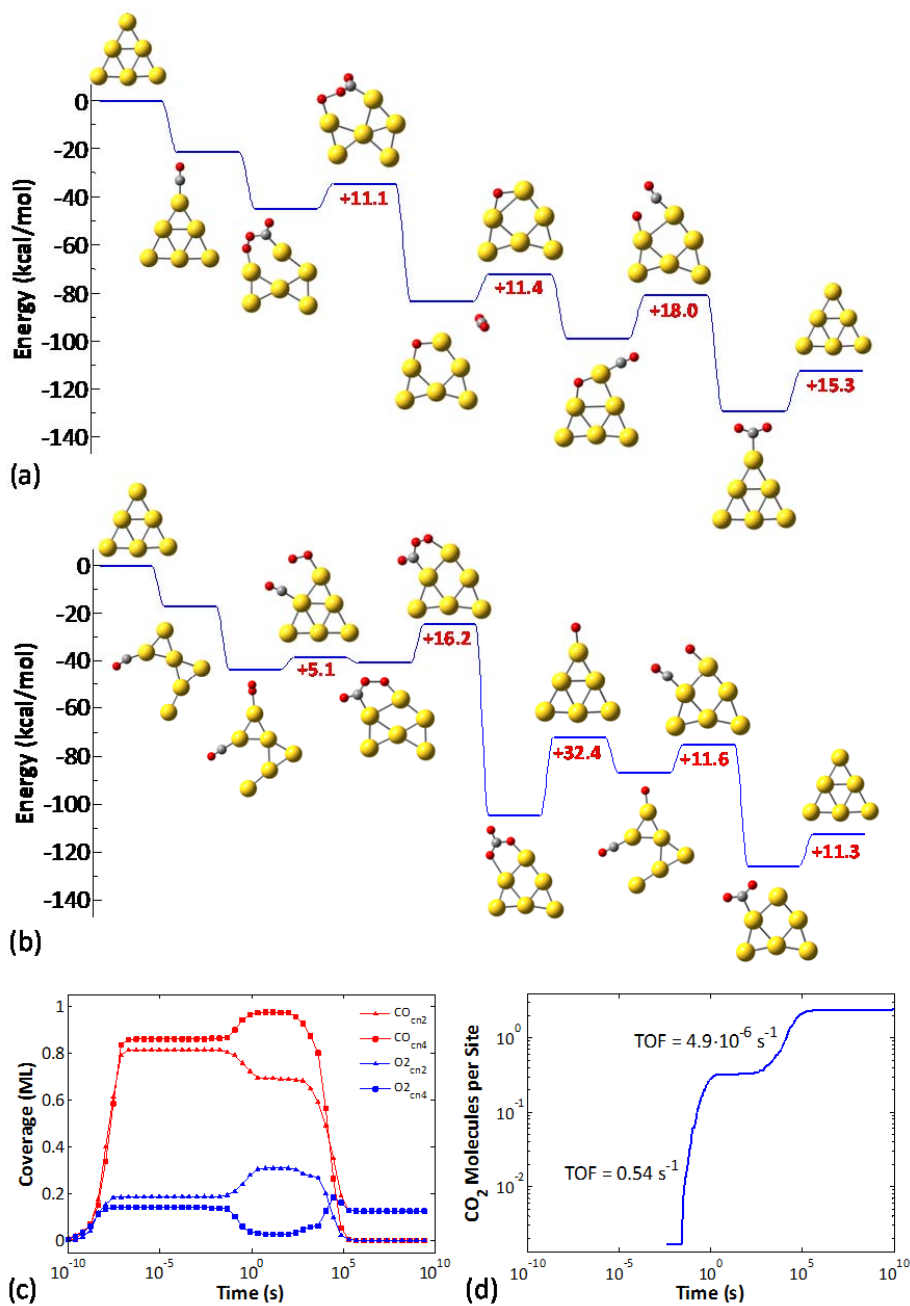


Figure 6: (a) Unhindered CO oxidation pathway on the Au_6^- nanocluster, with CO initially adsorbing on a CN2 site and O_2 on a CN4 site. (b) The pathway resulting to poisoning on the Au_6^- nanocluster; here, CO initially adsorbs on a CN4 site and O_2 on a CN2 site. (c) Average coverages of CO and O_2 on the CN2 and CN4 sites of the Au_6^- nanocluster, calculated from an ensemble of 100 clusters (100 KMC runs with different random seed). (d) Average number of CO_2 molecules produced per cluster in an ensemble of 100 clusters. After exhibiting some transient activity Au_6^- is poisoned (see also Ref.⁴⁶).

For Au_6^- our previous work identified two possible pathways depending on the initial binding sites of O_2 and CO (Figure 6a, b),⁴⁶ both of which are active in different timescales: the contribution of each pathway is revealed by Figure 6c, which depicts the CO and O_2 coverages on the different site types of the Au_6^- cluster (all data are averages over an ensemble of 100 KMC runs), as well as Figure 6d which shows the CO_2 molecules produced per site. Evidently, there are two phases of transient activity, followed by the eventual poisoning of the cluster. Thus, initially, CO and O_2 are randomly adsorbing on the CN2 and CN4 sites, resulting in approximately same coverages for both site types. At timescales of around 10^{-2} s, the CO oxidation reaction initiates and proceeds via the first pathway (Figure 6a), as evidenced by the depletion of CO on CN2 and O_2 on CN4. Subsequently, on the timescale of 1 s, the second pathway becomes active (Figure 6b). This delay can be attributed to the slightly higher barriers thereof: 5.1 kcal/mol for the 4-center intermediate formation, and 16.2 kcal/mol for the conversion of the latter to CO_3 (in the first pathway the higher barrier is 18 kcal/mol for the final $\text{O}+\text{CO}$ reaction). CO_3 formation via the 2nd pathway competes with the 1st pathway, this is why we still see CO_2 formation even well after 1 s. Note that the plateau in the CO_2 produced in the in the log-log diagram of Figure 6d is due to the distortion of timescales in the logarithmic scale: short timescales are magnified and long timescales shrink. Plotted in linear scale, it is apparent that CO_2 formation does not cease temporarily to resume with higher rates later; it proceeds continuously, but with a much lower rate after about 1 s. Eventually, the catalyst gets poisoned by CO_3 : the non-zero average coverages for O_2 at CN4 and CO at CN2 are due to the nanoclusters with 2 CO_3 molecules in the opposite sides of the triangular Au_6 structure.

Au_8^- on the other hand was found to exhibit the highest reactivity among the three clusters investigated (Figure 7). The reaction proceeds via the formation and decomposition of a four-center $\text{CO}\cdots\text{O}_2$ intermediate. Two pathways contribute to the overall activity: the first one involves a monodentate binding configuration of the four-center intermediate, whose decomposition according to step (b) of Figure 3 is rate limiting. The second pathway implicates a bidentate configuration and entails adsorbate-induced cluster reconstruction. The latter was taken into account implicitly in the energetics of the reaction steps. Notice that this cluster reconstruction is induced by the adsorption of the reacting species and not by the symmetry of the cluster as we showed in Figure 5. The average turnover frequency (TOF) of this cluster was estimated to 0.73 s^{-1} and was the highest among those of the Au nanoclusters considered.

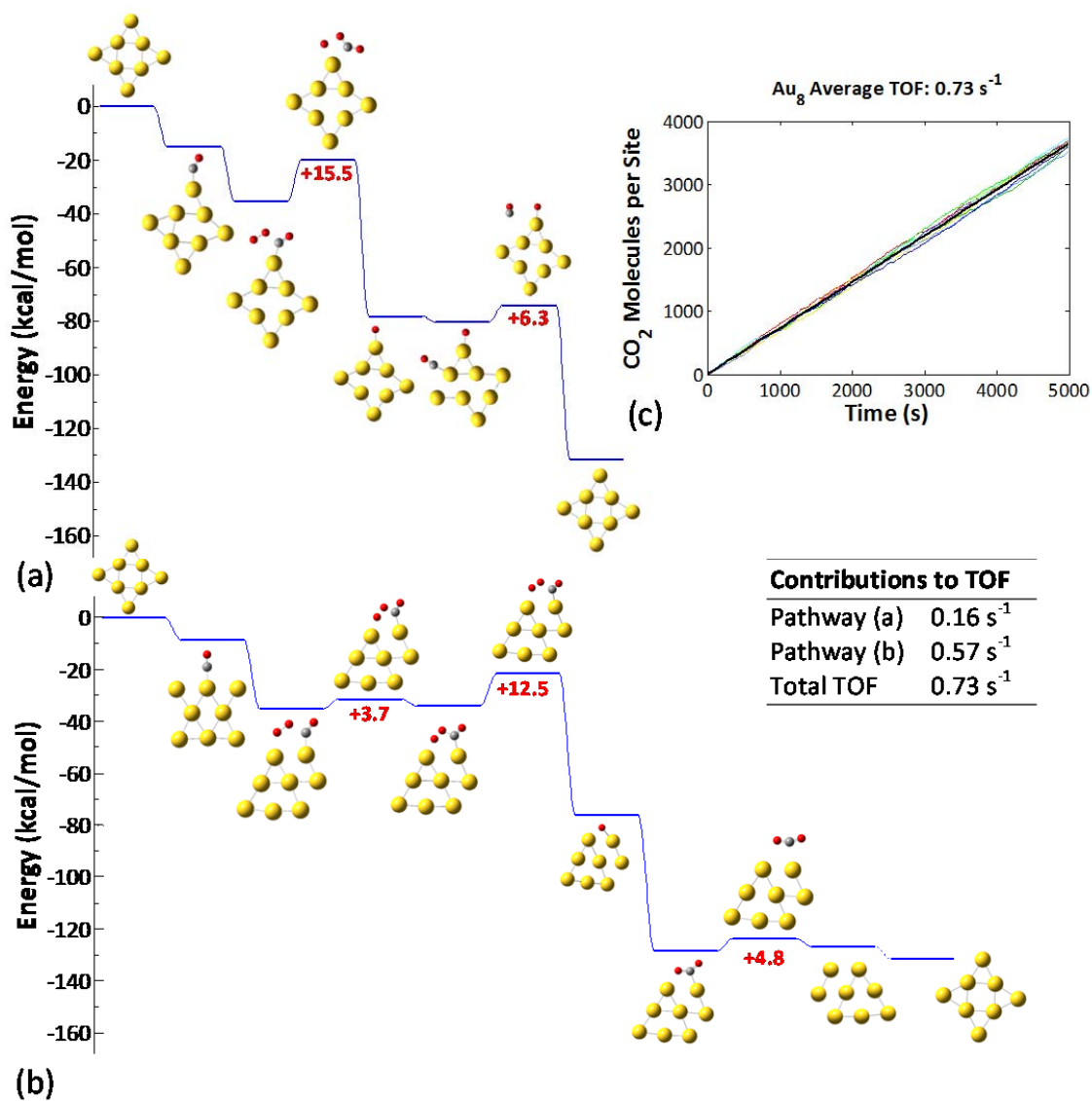


Figure 7: (a, b) Kinetically preferred pathways on Au_8^- . (c) Number of CO_2 molecules produced per site in an ensemble of 10 clusters; the average number is denoted by the thick black line. The contributions of the two pathways on the overall TOF are noted.

In the case of Au_{10}^- , bidentate O_2 species were found to be significantly more stable than monodentate ones (by about 10 kcal/mol); however, the former are inactive due to the high barriers of the reaction with CO^{38} . Thus, on the Au_{10}^- structure, the chemistry proceeds via the tilting of bidentate O_2 to a monodentate (active) configuration (Figure 8a), followed by the

reaction between O_2 and adsorbed CO, which has an activation energy on the order of 10 kcal/mol (the exact values depend on the actual sites occupied and are shown in the supplementary information file). The sequence of these two steps is rate-limiting for the CO oxidation reaction on Au_{10}^- . The TOF of this cluster is approximately 0.02 s^{-1} (Figure 8b), which is lower than that of Au_8^- by more than an order of magnitude and in qualitative agreement with experimental observations (Au_6^- inert, Au_8^- active, Au_{10}^- less active than Au_8^-)²⁸⁻³⁰.

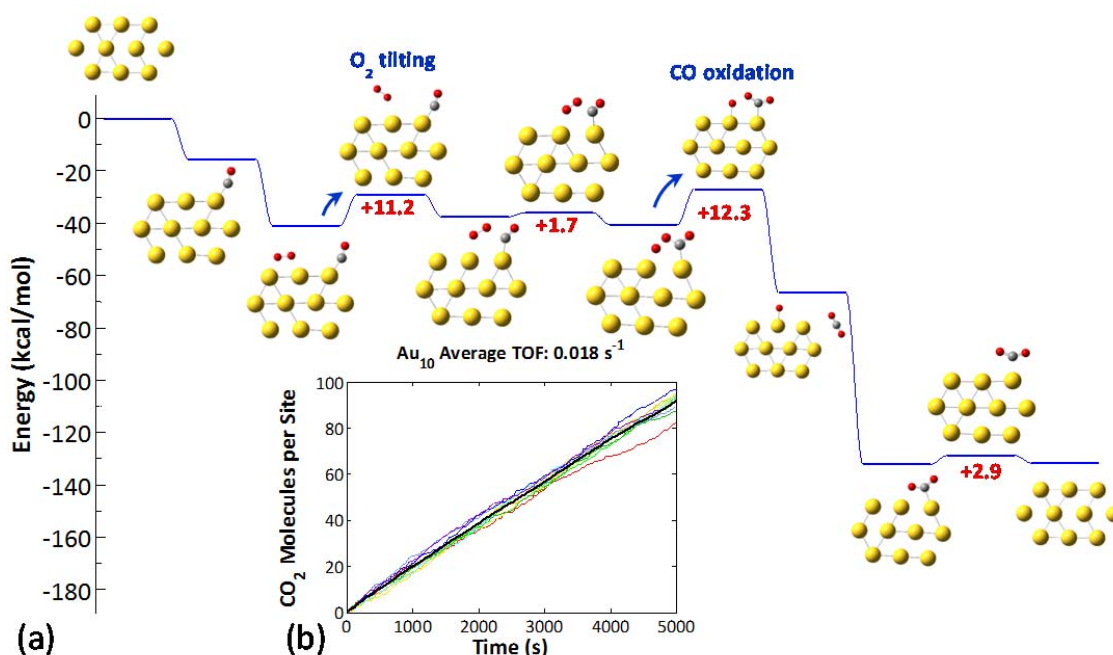


Figure 8: (a) Representative kinetically favored CO oxidation pathway on Au_{10}^- . (b) Number of CO_2 molecules produced per site in an ensemble of 10 clusters; the average number is denoted by the thick black line.

As a final note, this work highlights that more sophisticated models need to be developed to correlate the catalytic activity with electronic properties of the clusters, which in turn arise from their geometric characteristics^{48, 49}. In addition, the stability of the supported clusters plays an important role on their catalytic behavior. Incorporation of ligands on Au clusters could improve their stability by limiting cluster agglomeration, while maintaining CO oxidation activity¹. However, the reaction mechanisms on these clusters are expected to completely change in the presence of ligands.

Conclusions

Using multiscale modeling simulations we investigated the CO oxidation behavior of subnanosized Au catalysts that consist of a few metal atoms. This study unravels a high degree of complexity in the catalytic behavior of Au clusters: competing physicochemical phenomena on the catalyst result to the experimentally observed “magic number” CO oxidation activity. Subnanocatalysis, despite being attractive due to the atomic-level precision of the catalysts and its often unprecedented performance, remains an empirical field. Simulations, such as the ones presented here, can significantly advance our understanding and lead to better catalysts and processes.

Acknowledgements

G.M. and N.A. would like to acknowledge computational support from the Center for Simulation and Modeling (SAM) and start-up funding from the University of Pittsburgh. M.S. acknowledges the use of the UCL Legion High Performance Computing Facility (Legion@UCL), and associated support services, in the completion of the KMC simulations of this work. The material on CO oxidation on Au is also based upon work financially supported by a Marie Curie International Outgoing Fellowship within the 7th European Community Framework Programme. The work conducted at Delaware was supported by Grant No. DE-SC0010549 from the (U.S.) Department of Energy (DOE).

Author Contributions: N.N., N.A., M.S. and G.M. performed the calculations. G.M., M.S. and D.G.V. conceptualized the study and carried out the advising. G.M. and M.S. wrote the manuscript and all authors edited and proofread the paper.

References

1. O. Lopez-Acevedo, K. A. Kacprzak, J. Akola and H. Hakkinen, *Nature Chemistry*, 2010, 2, 329-334.
2. Q. Fu, H. Saltsburg and M. Flytzani-Stephanopoulos, *Science*, 2003, 301, 935-938.
3. M. Valden, X. Lai and D. W. Goodman, *Science*, 1998, 281, 1647-1650.
4. B. Hammer and J. K. Norskov, *Nature*, 1995, 376, 238-240.
5. J. Quilter, *Science*, 1998, 282, 1058-1059.
6. G. C. Bond and D. T. Thompson, *Catalysis Reviews-Science and Engineering*, 1999, 41, 319-388.
7. G. Mpourmpakis, S. Caratzoulas and D. G. Vlachos, *Nano Letters*, 2010, 10, 3408-3413.

8. P. D. Jadzinsky, G. Calero, C. J. Ackerson, D. A. Bushnell and R. D. Kornberg, *Science*, 2007, 318, 430-433.
9. Y. G. Sun and Y. N. Xia, *Science*, 2002, 298, 2176-2179.
10. E. Boisselier and D. Astruc, *Chem. Soc. Rev.*, 2009, 38, 1759-1782.
11. M. Haruta, T. Kobayashi, H. Sano and N. Yamada, *Chemistry Letters*, 1987, 16, 405-408.
12. T. S. Kim, J. D. Stiehl, C. T. Reeves, R. J. Meyer and C. B. Mullins, *Journal of the American Chemical Society*, 2003, 125, 2018-2019.
13. W. S. Epling, G. B. Hoflund, J. F. Weaver, S. Tsubota and M. Haruta, *Journal of Physical Chemistry*, 1996, 100, 9929-9934.
14. S. D. Lin, M. Bollinger and M. A. Vannice, *Catalysis Letters*, 1993, 17, 245-262.
15. B. Schumacher, V. Plzak, M. Kinne and R. J. Behm, *Catalysis Letters*, 2003, 89, 109-114.
16. J. D. Stiehl, T. S. Kim, S. M. McClure and C. B. Mullins, *Journal of the American Chemical Society*, 2004, 126, 13574-13575.
17. S. Tsubota, D. A. H. Cunningham, Y. Bando and M. Haruta, in *Preparation of Catalysts Vi*, 1995, vol. 91, pp. 227-235.
18. M. Haruta, *Cattech*, 2002, 6, 102-115.
19. R. Meyer, C. Lemire, S. K. Shaikhtudinov and H. Freund, *Gold Bulletin*, 2004, 37, 72-124.
20. D. R. Rainer and D. W. Goodman, *Journal of Molecular Catalysis a-Chemical*, 1998, 131, 259-283.
21. M. C. Kung, R. J. Davis and H. H. Kung, *Journal of Physical Chemistry C*, 2007, 111, 11767-11775.
22. G. C. Bond, C. Louis and D. T. Thompson, *Catalysis by Gold*, Imperial College Press, 2006.
23. B. Hvolbaek, T. V. W. Janssens, B. S. Clausen, H. Falsig, C. H. Christensen and J. K. Norskov, *Nano Today*, 2007, 2, 14-18.
24. G. Mpourmpakis, A. N. Andriotis and D. G. Vlachos, *Nano Letters*, 2010, 10, 1041 - 1045.
25. I. N. Remediakis, N. Lopez and J. K. Norskov, *Applied Catalysis a-General*, 2005, 291, 13-20.
26. I. X. Green, W. Tang, M. Neurock and J. T. Yates, Jr., *Science*, 2011, 333, 736-739.
27. T. Fujitani and I. Nakamura, *Angewandte Chemie-International Edition*, 2011, 50, 10144-10147.
28. A. Sanchez, S. Abbet, U. Heiz, W. D. Schneider, H. Hakkinen, R. N. Barnett and U. Landman, *Journal of Physical Chemistry A*, 1999, 103, 9573-9578.
29. B. Yoon, H. Hakkinen, U. Landman, A. S. Worz, J.-M. Antonietti, S. Abbet, K. Judai and U. Heiz, *Science*, 2005, 307, 403-407.
30. M. Arenz, U. Landman and U. Heiz, *ChemPhysChem*, 2006, 7, 1871-1879.
31. G. Mills, M. S. Gordon and H. Metiu, *Chemical Physics Letters*, 2002, 359, 493-499.
32. S. Chretien, S. K. Buratto and H. Metiu, *Curr. Opin. Solid State Mat. Sci.*, 2007, 11, 62-75.
33. R. Pal, L. M. Wang, Y. Pei, L. S. Wang and X. C. Zeng, *Journal of the American Chemical Society*, 2012, 134, 9438-9445.
34. G. Li and R. C. Jin, *Accounts Chem. Res.*, 2013, 46, 1749-1758.

35. X. Guo, G. Fang, G. Li, H. Ma, H. Fan, L. Yu, C. Ma, X. Wu, D. Deng, M. Wei, D. Tan, R. Si, S. Zhang, J. Li, L. Sun, Z. Tang, X. Pan and X. Bao, *Science*, 2014, 344, 616-619.
36. R. Ahlrichs, M. Bar, M. Haser, H. Horn and C. Kolmel, *Chemical Physics Letters*, 1989, 162, 165-169.
37. M. J. T. Frisch, G. W.; Schlegel, H. B.; Scuseria, G. E.; Robb, M. A.; Cheeseman, J. R.; Scalmani, G.; Barone, V.; Mennucci, B.; Petersson, G. A.; Nakatsuji, H.; Caricato, M.; Li, X.; Hratchian, H. P.; Izmaylov, A. F.; Bloino, J.; Zheng, G.; Sonnenberg, J. L.; Hada, M.; Ehara, M.; Toyota, K.; Fukuda, R.; Hasegawa, J.; Ishida, M.; Nakajima, T.; Honda, Y.; Kitao, O.; Nakai, H.; Vreven, T.; Montgomery, Jr., J. A.; Peralta, J. E.; Ogliaro, F.; Bearpark, M.; Heyd, J. J.; Brothers, E.; Kudin, K. N.; Staroverov, V. N.; Kobayashi, R.; Normand, J.; Raghavachari, K.; Rendell, A.; Burant, J. C.; Iyengar, S. S.; Tomasi, J.; Cossi, M.; Rega, N.; Millam, J. M.; Klene, M.; Knox, J. E.; Cross, J. B.; Bakken, V.; Adamo, C.; Jaramillo, J.; Gomperts, R.; Stratmann, R. E.; Yazyev, O.; Austin, A. J.; Cammi, R.; Pomelli, C.; Ochterski, J. W.; Martin, R. L.; Morokuma, K.; Zakrzewski, V. G.; Voth, G. A.; Salvador, P.; Dannenberg, J. J.; Dapprich, S.; Daniels, A. D.; Farkas, Ö.; Foresman, J. B.; Ortiz, J. V.; Cioslowski, J.; Fox, D. J. Gaussian, Inc., Wallingford CT, 2009.
38. N. Nikbin, G. Mpourmpakis and D. G. Vlachos, *Journal of Physical Chemistry C*, 2011, 115, 20192-20200.
39. A. Prestianni, A. Martorana, F. Labat, I. Ciofini and C. Adamo, *Journal of Physical Chemistry B*, 2006, 110, 12240-12248.
40. T. Davran-Candan, A. E. Aksoylu and R. Yildirim, *Journal of Molecular Catalysis a-Chemical*, 2009, 306, 118-122.
41. M. Stamatakis, *Zacros: Advanced Lattice-KMC simulation Made Easy*, <http://tinyurl.com/zacroskmc>.
42. M. Stamatakis and D. G. Vlachos, *Journal of Chemical Physics*, 2011, 134, 214115.
43. J. Nielsen, M. d'Avezac, J. Hetherington and M. Stamatakis, *J. Chem. Phys.*, 2013, 139, 224706.
44. M. Stamatakis and D. G. Vlachos, *ACS Catal.*, 2012, 2, 2648-2663.
45. A. Chatterjee and D. G. Vlachos, *Journal of Computer-Aided Materials Design*, 2007, 14, 253-308.
46. M. Stamatakis, M. A. Christiansen, D. G. Vlachos and G. Mpourmpakis, *Nano Letters*, 2012, 12, 3621-3626.
47. K. McKenna, T. Trevethan and A. Shluger, *Physical Review B*, 2010, 82.
48. H. Li, L. E. Li and Y. D. Li, *Nanotechnol. Rev.*, 2013, 2, 515-528.
49. J. Liu, K. S. Krishna, Y. B. Losovyj, S. Chattopadhyay, N. Lozova, J. T. Miller, J. J. Spivey and C. Kumar, *Chem.-Eur. J.*, 2013, 19, 10201-10208.